

On the Relevance of $\ln(z_0/z_{0T}) = kB^{-1}$

Bruce B. Hicks¹ · William R. Pendergrass² · Barry D. Baker³ · Rick D. Saylor² · Debra L. O'Dell⁵ · Neal S. Eash⁵ · Jeffrey T. McQueen⁴

Received: 1 February 2017 / Accepted: 2 November 2017 / Published online: 22 November 2017
© The Author(s) 2017. This article is an open access publication

Abstract The assumption that the roughness Reynolds number (Re_*) can be used as a basis for quantifying the boundary-layer property kB^{-1} ($= \ln(z_0/z_{0T})$) as in some modern numerical models is questioned. While Re_* is a useful property in studies of pipe flow, it appears to have only marginal applicability in the case of treeless terrain, as studied in the two experimental situations presented here. For both the daytime and night-time cases there appears to be little correlation between kB^{-1} and Re_* . For daytime, the present studies indicate that the assumption $kB^{-1} \approx 2$ is acceptable, while for night-time, the scatter involved in relating kB^{-1} to Re_* suggests there is little reason to assume a direct relationship. However, while the scatter affecting all of the night-time results is large, there remains a significant correlation between the heat and momentum fluxes upon which an alternative methodology for describing bulk air–surface exchange at night could be constructed. The friction coefficient (C_f) and the turbulent Stanton number (St_*) are discussed as possible alternatives for describing bulk properties of the air layer adjacent to the surface. While describing the surface roughness in terms of the friction coefficient provides an attractive simplification relative to the conventional methodologies based on roughness length and stability considerations, use of the Stanton number shares many of uncertainties that affect kB^{-1} . The transitions at dawn and dusk remain demanding situations to address.

✉ Bruce B. Hicks
hicks.metcorps@gmail.com

¹ Metcorps, P.O. Box 1510, Norris, TN 37828, USA

² Atmospheric Turbulence and Diffusion Division, Air Resources Laboratory, National Oceanic and Atmospheric Administration, P.O. Box 2456, Oak Ridge, TN 37830, USA

³ Air Resources Laboratory, National Oceanic and Atmospheric Administration, 5830 University Research Court, College Park, MD 20740, USA

⁴ National Centers for Environmental Prediction, National Oceanic and Atmospheric Administration, 5830 University Research Court, College Park, MD 20740, USA

⁵ Biosystems Engineering and Soil Science, Institute of Agriculture, University of Tennessee, Knoxville, TN 37996, USA

Keywords Atmospheric surface boundary layer · kB^{-1} · $\ln(z_0/z_{0T})$ · Roughness lengths · Stanton number

1 Introduction

A review of the formulations used in modern mesoscale (and other) models reveals that the assumptions are sometimes at variance with current understanding. The consequences are not always apparent in model simulation results, sometimes because the differences in formulations are not great enough to be of major influence but also sometimes because of a tuning process that forces correspondence between predictions and observations for specific locations (e.g. Gong et al. 1998; Marzban et al. 2014). In the present discussion, the focus is on one particular example—the parametrization of kB^{-1} in descriptions of air–surface exchange. The issue arises in examination of proposed methods to use the thermal roughness length (z_{0T}) derived from consideration of the sensible heat flux and the bulk temperature difference between the surface and the air as a basis for atmospheric surface-layer and planetary boundary-layer (PBL) computations. These methods derive from experimental findings that z_{0T} differs from z_0 , the conventional aerodynamic roughness length associated with the wind profile (Owen and Thomson 1963; Plate 1971; Brutsaert 1982; Garratt 1992). The issue also arises in air pollution modelling. For example, a feature of contemporary models addressing small particle deposition is the prediction of the deposition velocity that differs from field experimental results (Gallagher et al. 1997; Garland 2001; Hicks et al. 2016). Inspection of the models reveals a common feature that potentially causes a depiction of the role of particle size differing substantially from reality—the depiction of the resistance associated with the quasi-laminar boundary layer, R_b . Both of the quantities R_b and kB^{-1} ($= \ln(z_0/z_{0T})$) relate to the extension of micrometeorological flux–gradient relationships towards the surface, where molecular-scale processes become important. The two quantities are closely connected, since

$$(u_0 - u_z) = (\overline{w'u'}/ku_*) (\ln(z/z_0) - \psi_m(\zeta)), \tag{1a}$$

or (more familiarly)

$$u_z = (u_*/k) (\ln(z/z_0) - \psi_m(\zeta)). \tag{1b}$$

Similarly

$$\begin{aligned} (T_0 - T_z) &= (\overline{w'T'}/ku_*) (\ln(z/z_{0T}) - \psi_H(\zeta)) \\ &= (\overline{w'T'}/ku_*) (\ln(z/z_0) + \ln(z_0/z_{0T}) - \psi_H(\zeta)). \end{aligned} \tag{2}$$

Here, notation follows that of the conventional Monin–Obukhov similarity theory (MOST), with $\zeta = z/L$, and where z is the height above the appropriate zero plane, L is the Obukhov length scale, u_* is the friction velocity, and T_z and u_z are the temperature and wind speed at height z . In neutral conditions, both ψ functions are zero. If the electrical analogy is adopted, the major resistances involved are the aerodynamic resistance (R_a), defined as

$$R_a = u_z/u_*^2 = (\ln(z/z_0) - \psi_m(\zeta))/(ku_*), \tag{3}$$

and a resistance associated with molecular-scale transfer across the layers of air adjacent to the receptor surface(s) (R_b), which in the case of heat exchange is defined as

$$R_b = (T_0 - T_z)/\overline{w'T'} - R_a. \tag{4}$$

A third resistance describing the chemical and/or biological composition and consequences of the surface is of relevance in the case of trace gas exchange: R_c . This surface or “capture” resistance is not of immediate relevance to the considerations of heat exchange that follow, although it does incorporate such factors as stomatal resistance, which are central considerations in the case of the evaporative heat exchange.

Equations 2 and 3 lead directly to an expression for R_b that parallels Eq. 3,

$$R_b = (\ln(z_0/z_{0T}) + \psi_m(\zeta) - \psi_H(\zeta)) / ku_*, \quad (5)$$

and following from flat-plate and pipe-flow studies, the quantity R_b is likened to the laminar-layer resistance of fluid mechanics. However, because a vegetated surface is made up of a large number of contributing surfaces, each of which must exhibit its own boundary-layer resistivity, R_b is conventionally referred to as the “quasi-laminar resistance,” a term originally proposed to emphasize this distinction. Constructing a general description of R_b in terms of an understanding of the characteristics of the individual roughness elements of the surface remains a challenge.

The roughness lengths z_0 and z_{0T} are quantities derived from wind-speed and temperature profiles measured well above the region of immediate influence of individual surface roughness elements. Relating either roughness length to actual physical features of the surface is also a continuing challenge. The relationship between z_0 and z_{0T} was explored in wind-tunnel studies by Owen and Thomson (1963) and in various analyses by, e.g., Chamberlain (1968, 1974). Garratt and Hicks (1973, hereafter G&H) extended the resulting formulations to the real world, by summarizing data from micrometeorological field studies as well as from physical modelling. Subsequent presentations by Garratt and Francey (1978) and Garratt (1992) refined the G&H analysis, with the focus on the dependence of $\ln(z_0/z_{0T}) = kB^{-1}$ on surface properties, represented by the roughness Reynolds number

$$Re_* = u_* z_0 / \nu. \quad (6)$$

Data obtained in studies of bluff objects in controlled conditions seemed to agree with Owen and Thomson (1963),

$$kB^{-1} = a(Re_*)^b \quad (7)$$

where $a \approx 0.6$ and $b \approx 0.45$. Figure 1 shows the data as plotted by G&H (the solid circles) and a number of descriptions of the kB^{-1} versus Re_* dependence derived from data obtained subsequently. In agreement with Chamberlain (1966), G&H emphasized that Re_* is a poor index for comparing fundamental characteristics of natural surfaces. Over much of the range likely to be found in real-world situations, the G&H results indicate that the appropriate value of kB^{-1} might best be

$$kB^{-1} \approx 2, \quad (8)$$

(see Garratt and Francey 1978).

Included in Fig. 1 are results from two recent studies conducted in widely dissimilar situations. The first study was over a field of grazed pasture in Alabama (Pendergrass et al. 2017), the other over a fallow field in the dry season of Zimbabwe (O’Dell et al. 2015; Hicks et al. 2015). The curves (1) through (4) plotted in Fig. 1 represent several different kB^{-1} versus Re_* relationships as listed by Chen et al. (2010) and as incorporated in many of today’s numerical models. All of these forms depart substantially from the recommendation by Garratt and Francey (1978) that site-averaged values of kB^{-1} approach a plateau as Re_* increases, $kB^{-1} \approx 2$, whereas the initial G&H interpretation of data then available was that

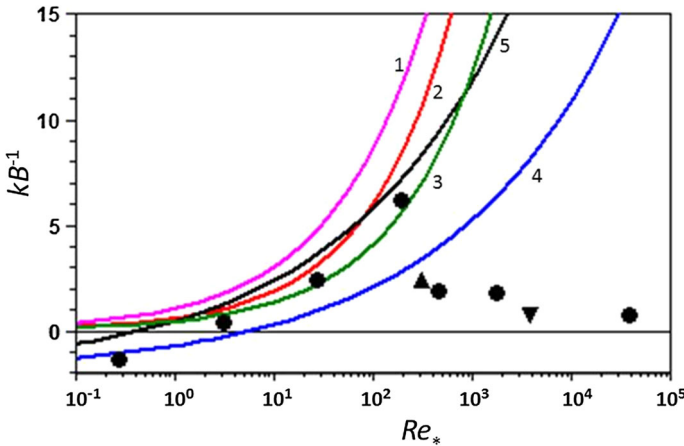


Fig. 1 The variation with surface roughness Reynolds number of the boundary-layer resistance factor $kB^{-1} = \ln(z_0/z_{0T})$, as determined for the case of heat transfer and as reported by G&H. The solid circles (●) represent the average results from datasets originally available to G&H. Two additional averages are plotted, both discussed below: black up-pointing triangle daytime results obtained over natural fallow in Zimbabwe, and black down-pointing triangle the average of daytime measurements made over grazed pasture in Alabama. The curves drawn are due to, (1) Zhang et al. (2001), (2) Owen and Thomson (1963), (3) Brutsaert (1975), and (4) Kanda et al. (2007). Curve (5) has been created using random numbers

kB^{-1} decreases uniformly from a maximum value of about 2 at $Re_* = 10^2$ to about zero at $Re_* = 10^5$, much as might be concluded from Fig. 1.

A common feature of the individual datasets seen in Fig. 1 is that their component observations are highly scattered, often between the bounds represented by Eqs. 7 and 8. In this regard, it must be remembered that the original depiction (as by G&H) was influenced by the lack of field data obtained at night. In subsequent work, it has become apparent that nighttime data yield much more scatter than daytime, as must be expected because at night both $\overline{w'T'}$ and $|T_0 - T_z|$ are small and their ratio is therefore poorly determined. This issue was emphasized by, e.g., Stewart et al. (1994), Verhoef et al. (1997), and Yang et al. (2008), whose experiments revealed representative values of kB^{-1} that differed greatly from the depictions illustrated in Fig. 1. The vulnerability of the process by which values of z_{0T} and z_0 or any other characteristics of the surface are derived from field observations is well illustrated by Malhi (1996) whose analysis indicates values of z_{0T} in the range 10^{-7} to 10^{-11} m depending on the method of analysis. (For comparison, consider that the wavelength of visible light is $\sim 10^{-7}$ m.)

There are conceptual, as well as analytical, problems arising from the extension of the wind-tunnel dependence of kB^{-1} on Re_* to the real world. In particular, the association of viscosity (ν , at the molecular level) with u_* and z_0 (both meteorological quantities appropriate for a landscape) strains credibility. G&H proposed that some other parameter might be of more use in ordering the variability in kB^{-1} , and Garratt et al. (1993) emphasized that any such analysis requires direct measurement of the infrared surface temperature and is inevitably susceptible to uncertainties associated with the friction velocity. Verhoef et al. (1997) take the matter further and conclude that, in practice, kB^{-1} is an inappropriate index to use. Some contemporary models make use of Eq. 7 to derive grid-cell representative values of kB^{-1} , others rely on the constancy described by Eq. 8 [e.g. the Community Multiscale Air Quality (CMAQ) model, <https://www.cmascenter.org/cmaq/>].

2 A Simple Credibility Check

The problems associated with normalizing variables and with the subsequent association of one normalized variable with another (see Hicks 1978) generate uncertainty about any proposed relationship between kB^{-1} and Re_* , since each of these two quantities depends on both z_0 and u_* . To test the vulnerability of analyses yielding data like those depicted in Fig. 1, a body of daytime pseudo-data was developed, using a random number generator. As was the case in the original G&H analysis, the focus was on the temperature regime rather than on gases or particles. The distributions of independent random numbers were bounded by 0.02 and 0.92 m s⁻¹ for u_* , 5 and 300 W m⁻² for the sensible heat flux H , 0.005 and 0.9 m for z_0 . To lock the data into some similarity with reality, an average value of the thermal conductivity was assumed: $k_T = H/(\rho c_p(T_0 - T_z)) \approx 0.01$ m s⁻¹, but this was allowed to vary around the average. The property k_T is analogous to the familiar deposition velocity for airborne pollutants, with T_0 being the surface temperature value and T_z the air temperature. From these “data,” values of kB^{-1} and Re_* were derived using the following relationship, derived by manipulation of Eqs. 1 and 2,

$$\ln(z_0/z_{0T}) = ku_*(T_0 - T_z)/\overline{w'T'} - ku/u_* + (\psi_H - \psi_m), \quad (9)$$

and where the stability functions ψ_H and ψ_m were quantified using published relationships (Paulson 1970). The results from a set of 500 cases were then subjected to a power-law regression. The results must depend on the distribution of random numbers generated for each group, and hence many such tests were conducted with overall consequences that appear to mimic Eq. 7: $a = 0.46 \pm 0.06$, and $b = 0.47 \pm 0.02$. In comparison, the original analysis by Owen and Thomson (as mentioned above) yielded $a = 0.6$ and $b = 0.45$. Many of the alternative expressions listed by Yang et al. (2008) share the assumption that $b = 0.5$. The black line in Fig. 1 shows the result of the present random number analysis; it is clear that the black line is a close approximation to several of the proposed relationships.

3 Recent Field Data

Analysis of actual observations serves to emphasize the difficulties that arise when relying on assumed relationships between kB^{-1} and Re_* . Figure 2 illustrates results obtained from analysis of two recent datasets. The first study (“ZIM”) uses data obtained in an investigation of the benefits of alternative agricultural practices, conducted near Harare, Zimbabwe (O’Dell et al. 2015). Measurements were made of infrared surface temperature, air temperature (at 1 m), variances and covariances ($z = 2.4$ m, using sonic anemometry) over a poorly-vegetated flat field. The second study (“BAMA”) investigated convective initialization at an experimental station near Huntsville, Alabama (Pendergrass et al. 2017). As in the Zimbabwe case, infrared surface temperatures were measured as well as assorted micrometeorological quantities (at 2 and 10 m). The ZIM results used here are for the Southern Hemisphere in September and October, 2015, and the BAMA results are for the Northern Hemisphere in September and October, 2014. Data points represent 30-min averages for the ZIM data, and 15-min averages for the BAMA. The two sites are quite different—the former was left fallow with uncultivated native growths (weeds) at an altitude of about 1500 m a.s.l., while the latter was unmanaged but grazed pasture at an altitude of about 500 m a.s.l. The ZIM site was characteristic of its surroundings, these being arid/fallow during the dry season and farmed sporadi-

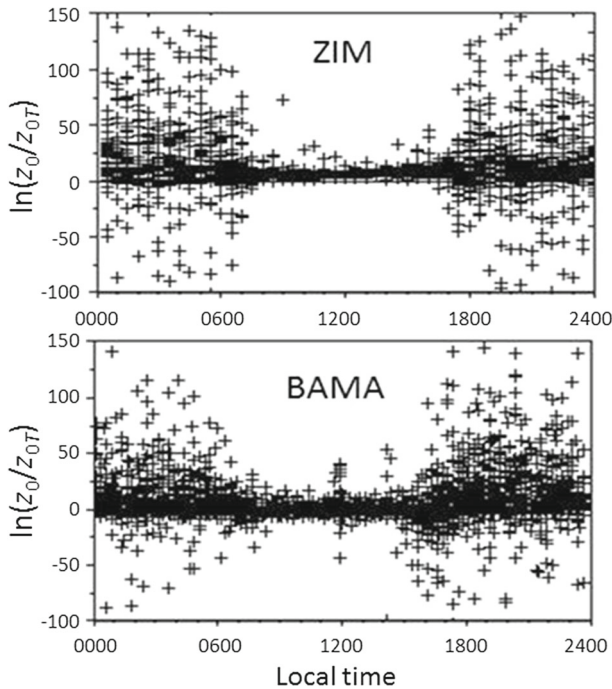


Fig. 2 Scatter diagrams showing the distribution by local standard time of $kB^{-1} = \ln(z_0/z_{0T})$ derived from field studies in Zimbabwe and Alabama, September and October in 2015 (ZIM) and 2014 (BAMA)

cally at the subsistence level during the rainy season. The BAMA location is surrounded by actively managed agriculture, with varying characteristics in soil type, size, and crop.

Using Eq. 9, the reported measurements enable computation of the property $\ln(z_0/z_{0T})$, and in this real-world case night-time data are included. Note that in the night-time case the stability functions become largely irrelevant since the operative term is then the difference $(\psi_H - \psi_m)$ and in stable conditions the convention is that $\psi_H = \psi_m$. Despite this, the difficulties central to any assumption regarding the association of kB^{-1} with Re_* are compounded by the difference between daytime and night-time that is strikingly evident in Fig. 2. This diagram shows the distribution by time of day of $kB^{-1} = \ln(z_0/z_{0T})$ derived from field studies now considered. Data points represent 30-min averages for the ZIM data, and 15-min for the BAMA data. The dominant characteristics evident in Fig. 2 are the scatter of night-time data and the apparent constancy of the daytime.

Figure 3 presents BAMA and ZIM data as averaged diurnal cycles derived from two 2-month periods: July and August, and September and October. The error bounds plotted represent \pm one standard error on the averages, where each average comprises 25 data points, so the standard deviations are five times the error margins illustrated. The ZIM results for daytime appear to reflect the consequences of the daily temperature cycle, peaking in the mid-afternoon and with minima near dusk and dawn. The BAMA data do not display this coherent behaviour, although similar minima are evident near dusk and dawn. For the daytime period, the BAMA data indicate that a single low value for $\ln(z_0/z_{0T})$ is a good approximation, while there is no obvious ordered behaviour for night-time.

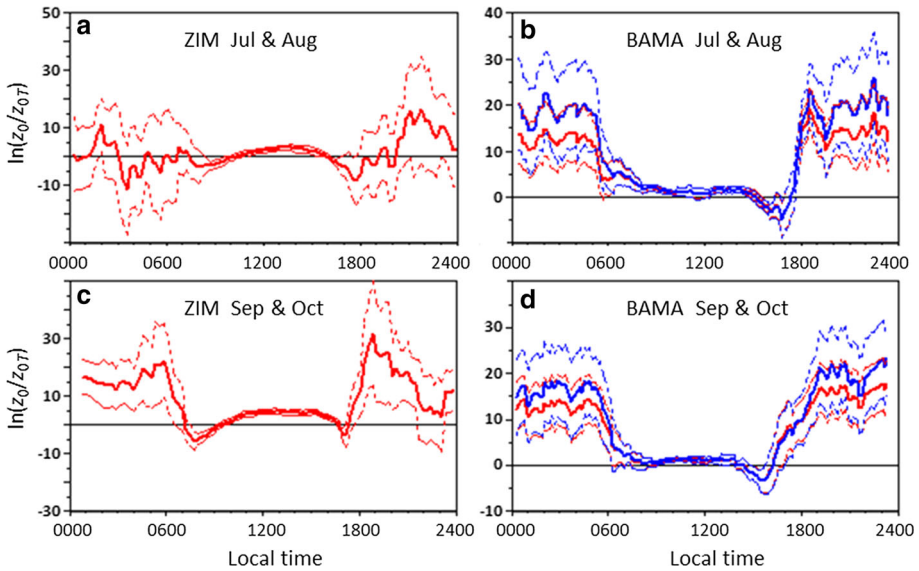


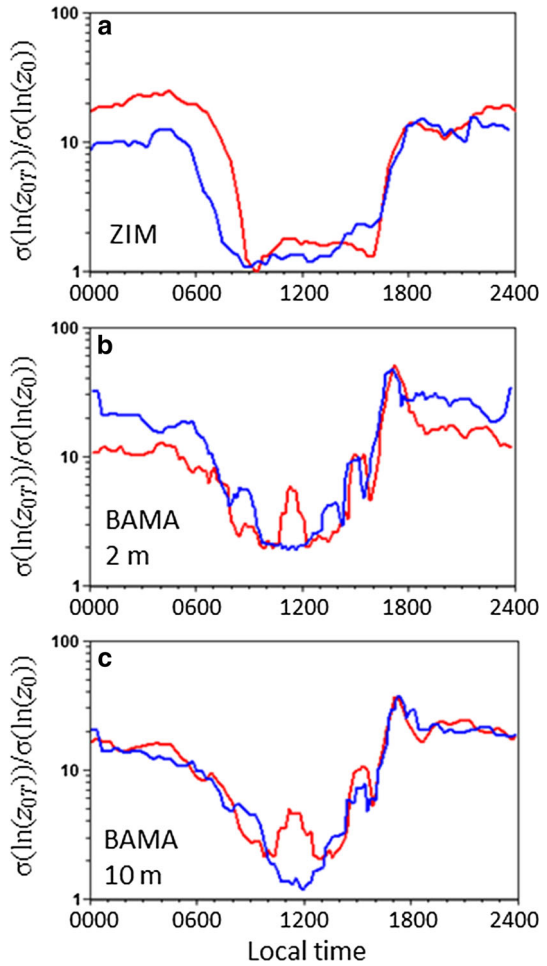
Fig. 3 Average diurnal cycles (local standard time) of $kB^{-1} = \ln(z_0/z_{0T})$ derived from the Zimbabwe and Alabama data, for two 2-month periods. The ZIM data were obtained in 2015, the BAMA data in 2014, in opposite seasonal periods (Southern Hemisphere for the former, Northern Hemisphere for the latter). Measurements from two heights are used to derive results for the BAMA dataset. The red plot represents results based on measurements at 2-m height, blue represents results based on 10-m data. Fine dotted lines depict the upper and lower bounds corresponding to \pm one standard error on the means

Between the daytime region of relative uniformity of kB^{-1} and the region of apparent randomness throughout the night, the transition periods near dusk and dawn present considerable conceptual difficulty. At these times, the sensible heat flux is small and varying with height as the depth of the mixed layer increases. Near-surface temperature gradients are also small and the roughness length z_{0T} is poorly determined.

Figure 3 also shows that the ZIM data for July and August can be represented, on the average, by a constant value throughout. This is not the case for September and October dataset, the results from which more closely resemble the BAMA results. The Zimbabwe dry season extended into October, and was broken with the arrival of seasonal rains (totalling 7.4 mm for October) during the middle of the month. The landscape subsequently adopted a greener and more heterogeneous appearance, so that irregularities are viewed as likely contributors to the differences affecting the upper left panel of Fig. 3. In this regard, the BAMA site can be characterized as the better site but in surroundings of more complex surface cover, whereas the ZIM site is the poorer site but is located in a widespread similar landscape.

Determination of the terms $\ln(z_0)$ and $\ln(z_{0T})$ is intermediate in the derivation of $\ln(z_0/z_{0T})$. In the present analytical procedure, groupings of observations according to time of day permit comparison of the statistical distributions of both of these key terms. The ratio of their standard deviations is an indication of their relative contribution to the scatter evident in Fig. 3. Values of this ratio are plotted in Fig. 4, showing a substantial difference between the ZIM and BAMA results, the former displaying more daytime order than the latter. However, both show that the source of the large scatter evident for night-time conditions lies with the description of the thermal exchange. For daytime conditions, the error margins associated

Fig. 4 Illustrations of the proportional attribution of scatter in the evaluation of $\ln(z_0/z_{0T})$ as illustrated in Fig. 3. In groupings of data ordered by time of day, standard deviations of the quantities $\ln(z_0)$ and $\ln(z_{0T})$ have been derived. The plots shown are of the ratios $\sigma(\ln(z_{0T}))/\sigma(\ln(z_0))$. Red indicates data for July and August; blue is for September and October

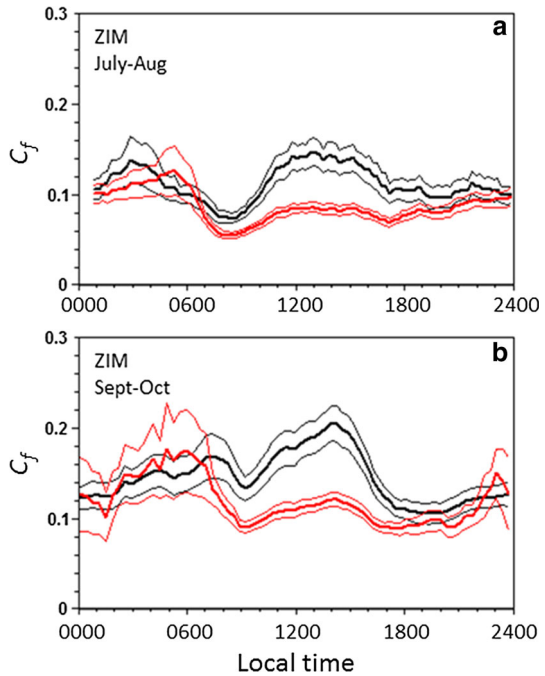


with the determination of z_{0T} are much like those for z_0 —the ratio of the standard deviations approaches unity. It is therefore evident that the scatter in $\ln(z_0/z_{0T})$ at night is due to either the measurements of the thermal contributing terms, the manner in which the effects of stability are accounted for, or some other characteristic of the night-time case that has yet to be identified.

4 Friction Coefficients and Stanton Numbers

In practice, the importance of the term kB^{-1} can be weighed by its relevance to the other terms in the principal relationships, primarily $\ln(z/z_0)$. For a most-common reference height $z = 10$ m (presumably above the relevant displacement height), it is then clear that the importance of the kB^{-1} term increases as the surface of interest becomes rougher. It is therefore expected that the areas most influenced by the acceptance (or otherwise) of relationships such as Eqs. 7 and/or 8 are urban areas and forests. The former may be argued to be better represented by

Fig. 5 The variation with time of day of the friction coefficient ($C_f = u_* / u$), for the ZIM dataset for September and October. The finer lines indicate \pm one standard error bounds. Black lines refer to raw data; red indicates results after correction for stability using conventional micrometeorology. The lines connect averages made up of 25 measurements each, grouped after ordering by time of day. Note that the standard deviations associated with individual measurements correspond to five times the standard error values evident here



Eq. 4, but not the latter (with the possible exception of coniferous forest canopies). The property of practical interest is the sum: $\ln(z/z_0) = \ln(z/z_0) + \ln(z_0/z_{0T})$. The value of the quantity $\ln(z/z_0)$ for a forested landscape and for a reference height of 10 m above the relevant zero plane is likely to be in the range 2 to 4, say 3. If one of the power-law relationships illustrated in Fig. 1 is used as a basis, then kB^{-1} can be estimated to be in the range 9–11, leading to an estimate of 15 for the desired quantity $\ln(z/z_{0T})$. On the other hand, acceptance of the Garratt and Francey (1978) recommendation of $\ln(z_0/z_{0T}) = 2$ results in a value of 5 for the same quantity. A factor of two or three in the consequent results would then seem likely. It is immediately clear that assuming a value of $\ln(z_0/z_{0T})$ that is too high will result in an overestimate of the resistance affecting sensible heat exchange. In passing, note that the 10-m reference level is adopted here because it is the common assumption of numerical simulations. This is despite the fact that the magnitude of the Obukhov length is frequently less than 10 m, hence causing a violation of the constraints originally imposed: that the flux–gradient relationships should not be extended beyond the range $-1 < z/L < 1$.

In the case of the momentum flux, the roughness characteristics of a reasonably flat landscape are conventionally defined using two variables, the zero-plane displacement, d , and the roughness length, z_0 . Both of these are likely to vary widely across any particular model grid cell. In practice the complexity can be reduced by considering the bulk association between the wind speed and the momentum loss at the surface; the quantity in question is the friction coefficient, $C_f \equiv u_* / u$. In simple concept, a map showing the spatial distribution of d and a second map showing z_0 could be replaced by a single map depicting C_f . However, the level of relevance would then need to be specified. In common contemporary applications, the height of relevance is often taken to be 10 m, but sometimes without acknowledgement that this refers, in turn, to a height of 10 m above the relevant zero plane.

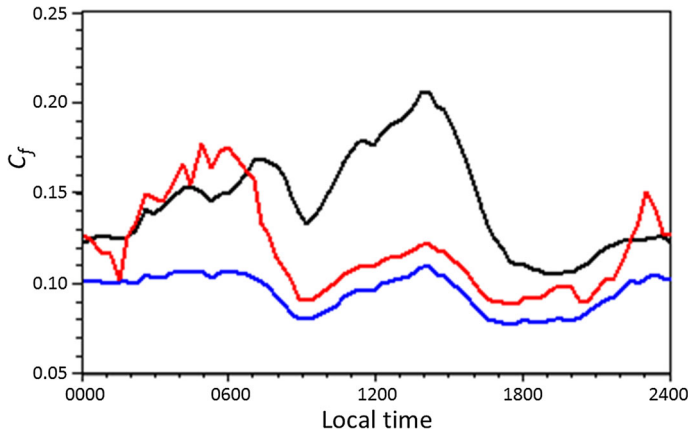


Fig. 6 The variation of C_f with time of day. The black line joins arithmetic averages of raw data. Red shows the results of correcting for stability, also using arithmetic averaging; blue shows the results if raw data are first transformed logarithmically, so that the blue line now joins geometric mean values. These results are based on the ZIM September and October dataset

Figure 5 presents C_f results from the ZIM study, showing that accounting for stability helps explain variations in the daytime: the standard errors associated with the average values plotted are reduced when stability corrections are applied and the magnitude of the variation in C_f through the daylight hours is also reduced. However, use of a stability correction does not seem to improve the night-time results. The causes are not clear, however the roles of measurement uncertainty and the methodology of the present analysis cannot be discounted. The friction coefficient is the ratio of two quantities that are individually highly variable at night, and hence analysis in terms of the logarithms of the ratio is preferred. That this is indeed the case is demonstrated in Fig. 6, where three friction coefficient determinations are plotted. The black line joins average values of u_*/u (as measured) after sorting by time of day; the red line joins the arithmetically-averaged C_f values after conventional correction for stability; the blue line shows the improved results if the stability-corrected values are averaged geometrically.

Just as the effective roughness of a landscape can be described by a friction coefficient (C_f) that is a slowly-varying characteristic of a surface, so its thermal exchange characteristics can be described by a heat conductivity—a turbulent equivalent to engineering's Stanton number. The discussion that follows centres on the turbulent Stanton number, $St_* = \overline{w'T'}/(u_*(T_0 - T_a))$, as initially discussed by Owen and Thomson (1963). This quantity differs from the conventional Stanton number of fluid dynamics by substituting the fluid velocity u by the scale velocity appropriate for turbulent exchange, u_* .

St_* shares the same variables that determine kB^{-1} , and so its night-time applicability should therefore be equally questionable. Figure 7 illustrates how St_* varies with time of day for two of the datasets considered above. Attention is immediately drawn to the dawn and dusk transition periods, which impose the need to consider the ratio $\overline{w'T'}/(T_0 - T_a)$ when both the numerator and denominator fluctuate around zero. The large excursions near dawn and dusk are therefore seen as likely artifacts of the analysis, and these periods are avoided in the discussion to follow. Inspection of Fig. 7a indicates that the ZIM data could be represented by two different plareau values for St_* , about 0.1 for daytime and about 0.02 for the night (computed so as to be appropriate for a 10-m reference height). If this result was

widely applicable, then a satisfactory response to modelling requirements could be to identify plateau regions such as those evident in Fig. 7a before and after each transition period, and to interpolate between them. In this way, the wide departures of St_* around and through neutral would be smoothed, diminishing greatly the consequences of the transitional variability.

Table 1 presents daytime and night-time average results derived from the six datasets considered here—ZIM, BAMA (2 m) and BAMA (10 m), each for two 2-month periods. The variables considered are $\ln(z_0/z_{0T})$, C_f , St_* and St , both as computed from raw data and after allowance for atmospheric stability. In every case, standard deviations are quoted as well as arithmetic averages, and to ensure that micrometeorological convention is not violated, occasions for which $|z/L| > 1.0$ have been excluded. Also omitted are occasions for which $|\overline{w'T'}| < 0.001 \text{ K m s}^{-1}$, and $|\overline{w'u'}| < 0.001 \text{ m}^2 \text{ s}^{-2}$. Although these data-selection criteria have been imposed to ensure a well-behaved dataset, the standard deviations evident in the Table remain large. (Note that standard deviations are listed in Table 1, whereas the standard errors on the mean are represented by the bounds shown in Figs. 3, 5, 7.)

The bold-face entries in Table 1 represent occasions in which a comparison between results derived using stability corrections and those that use raw data without such adjustment indicates reduced scatter. This identification is subjective, since the spread of contributing numbers from large negative to large positive (as is seen in Fig. 2) prohibits easy statistical examination. The daytime data indicate that in most cases it is better to use raw values, rather than values with stability corrections, especially in consideration of u_* . The night-time data indicate few cases for which such a preference can be identified. For example, the July–August night-time results indicate that C_f is better determined using the raw data, whereas the September–October results indicate the opposite.

The analysis so far has focussed on the turbulent Stanton number St_* , however the results shown in Table 1 indicate that the more conventional formulation (St) in which the friction velocity is replaced by the wind speed is often of equivalent statistical utility.

5 Discussion

The relevance of Re_* to a natural surface exposed to atmospheric turbulence presents a dilemma, since the role of Re_* arose from laboratory studies and a conceptual description of the processes involved, with a near-surface region of linear temperature gradient blending into a conventional micrometeorological logarithmic form (see Owen and Thomson 1963). The incorporation of the roughness length (z_0) was intended to represent the depth of the lowest part of the atmosphere within which the linear profiles dominated. However, there are few natural landscapes that would satisfy such criteria. G&H expressed doubt about the relevance of Re_* : “Thus, the behaviour must be influenced by some other surface consideration” and Verhoef et al. (1997) conclude that assuming a dependence of kB^{-1} on Re_* should be avoided if at all possible. Nevertheless, many modern models (air quality as well as meteorological) assume the broad applicability of Eq. 7, often with allowance for additional molecular diffusivity effects (through incorporation of the Schmidt number) if the application concerns air quality.

The present consideration of other descriptors of the surface (C_f , St and St_*) should be considered with careful attention to the way in which the same properties enter the relationships as are involved in determination of kB^{-1} . In practice, alternative approaches might prove to be better. Figure 8 shows that the night-time case could be addressed from an entirely different direction; the plots are of correlation coefficients among several pairs of variables.

Table 1 Average values of the friction coefficient (C_f), the Stanton number (St), the turbulent Stanton number (St_*) and kB^{-1} ($= \ln(z_0/z_{0T})$), for 6-h central daytime and nighttime periods (for the ZIM data –0900 to 1500 local time and 2100–0300 local time respectively; for the BAMA data, 0800–1400 and 2000–0400)

	Jul–Aug			Sep–Oct		
	ZIM 2 m	BAMA 2 m	BAMA 10 m	ZIM 2 m	BAMA 2 m	BAMA 10 m
<i>Raw data, daytime</i>						
C_f	0.180 (0.098)	0.165 (0.133)	0.126 (0.087)	0.150 (0.084)	0.158 (0.094)	0.119 (0.084)
St	0.013 (0.005)	0.027 (0.195)	0.019 (0.179)	0.008 (0.002)	0.020 (0.071)	0.009 (0.072)
St_*	0.093 (0.048)	0.120 (0.426)	0.207 (3.28)	0.061 (0.026)	0.126 (0.528)	0.107 (0.193)
<i>Stability-corrected, daytime</i>						
C_f	0.110 (0.040)	0.202 (0.311)	0.142 (1.516)	0.141 (0.081)	0.179 (0.477)	0.141 (0.751)
St	0.007 (0.046)	0.033 (0.390)	0.013 (0.002)	0.006 (0.002)	0.026 (0.155)	0.013 (0.027)
St_*	0.068 (0.169)	0.098 (3.094)	0.080 (0.016)	0.053 (0.017)	0.097 (1.190)	0.178 (0.568)
kB^{-1}	1.43 (3.77)	1.40 (3.33)	1.65 (0.40)	2.86 (6.72)	1.12 (2.72)	1.33 (0.40)
<i>Raw data, night</i>						
C_f	0.127 (0.071)	0.209 (0.272)	0.107 (0.193)	0.117 (0.066)	0.170 (0.209)	0.081 (0.065)
St	0.003 (0.005)	0.006 (0.032)	0.001 (0.027)	0.003 (0.003)	0.006 (0.007)	0.003 (0.003)
St_*	0.028 (0.037)	0.041 (0.307)	0.007 (0.324)	0.032 (0.029)	0.044 (0.051)	0.034 (0.040)
<i>Stability-corrected, night</i>						
C_f	0.129 (0.183)	0.144 (0.170)	0.083 (0.485)	0.115 (0.084)	0.124 (0.150)	0.057 (0.048)
St	0.005 (0.013)	0.003 (0.092)	0.004 (0.046)	0.003 (0.002)	0.006 (0.006)	0.002 (0.003)
St_*	0.005 (0.013)	0.035 (0.122)	0.005 (0.209)	0.032 (0.028)	0.040 (0.047)	0.022 (0.152)
kB^{-1}	4.57 (33.26)	12.57 (18.84)	18.03 (29.08)	12.07 (58.65)	12.43 (21.29)	15.82 (30.07)

Results obtained without accounting for the role of stability are given, together with the results obtained when stability corrections are made. Standard deviations are given in parentheses. Bold face indicates results that are more tightly confined in a comparison between raw data and stability corrected results, indicating an apparent preference

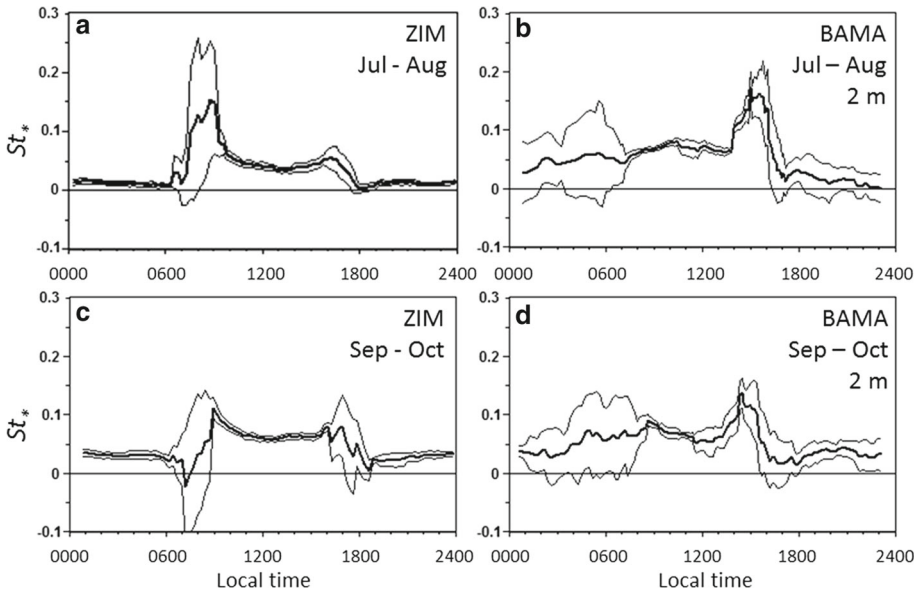


Fig. 7 The average variation with time of day of the turbulent Stanton numbers St_* for the two datasets considered here. The bounds indicate \pm one standard error on the means

Following conventional micrometeorological expectations, the plots show the associations between the fluxes of heat (Fig. 8a) and momentum (Fig. 8b) with corresponding pairs of state variables: the difference between the surface and the 10-m height of measurement [$(T_0 - T_{10})$ for Fig. 8a, and u_{10} for Fig. 8b], and the corresponding in-air differences ($(T_2 - T_{10})$, and $(u_{10} - u_2)$). Also shown (and identically in both Fig. 8a, b) is the correlation between the two eddy fluxes: $\overline{w'T'}$ and $\overline{w'u'}$. The figure shows the expected strong coupling between fluxes and in-air differences (gradients) for daytime conditions, with a correlation coefficient > 0.8 for most of the time. While the correlation for the bulk wind speed shown in Fig. 8b is almost the same as that for the wind-speed gradient in Fig. 8b, the corresponding plot for the surface-to-air temperature difference in Fig. 8a shows a substantially reduced correlation, indicating imperfections in the surface temperature observations. For night-time conditions, all of the correlations between fluxes and state variables are reduced, to levels such that reliance on them is likely to be unrewarding. This is in accord with the discussion of night-time kB^{-1} results above. However, while the associations between fluxes and gradients appear to be poor at night, the correlation coefficients between the two fluxes appear to remain high and are larger at night than in the daytime. An alternative path towards parametrizing the nocturnal case appears possible.

The preceding discussion emphasizes an issue that pervades all of the present considerations: in many numerical modelling schemes there is no accounting for the landscape variability of the relevant zero plane (of height d). If data are referred to a standard 10-m height, for example, the obvious question is “10 m above what?” The matter is of little practical relevance for sites such as those considered here (BAMA and ZIM), where the height of the vegetation is small in comparison to the 2-m measurement level. However, forested landscapes are common, and neglect of variations in d will then have consequences on the results of simulations although it is not obvious that the resulting uncertainties will be of concern.

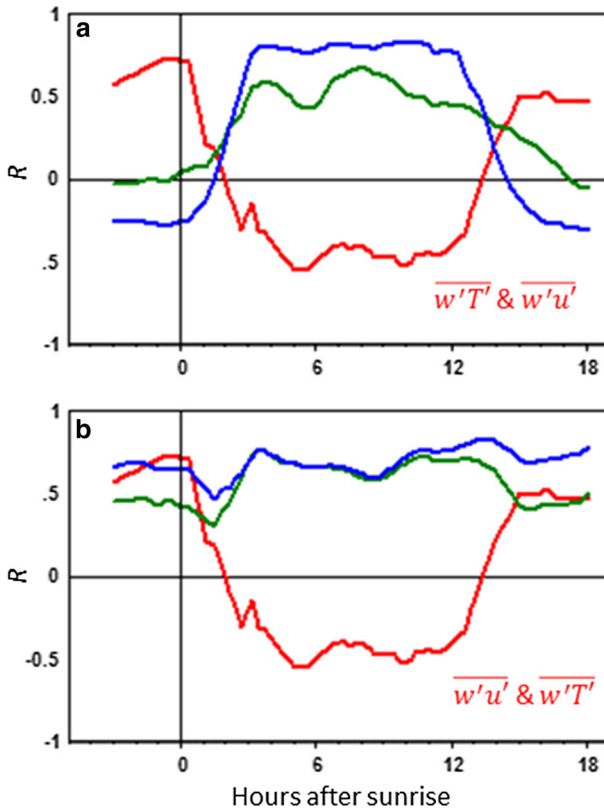


Fig. 8 Correlation coefficients (R) derived from associating different pairs of 15-min BAMA determinations of eddy fluxes and associated state variables. **a** $\overline{w'T'}$ is compared with $(T_0 - T_{10})$, with $(T_2 - T_{10})$, and with $-\overline{w'u'}$ (green, blue and red, respectively). **b** $-\overline{w'u'}$ is associated with u_{10} , $(u_{10} - u_2)$, and $\overline{w'T'}$ (green, blue and red, respectively)

6 Conclusions

The present intent is to draw attention to difficulties arising with common formulations of air–surface exchange, involving the surface roughness length index $kB^{-1} = \ln(z_0/z_{0T})$, as appears in some contemporary simulations. An erroneous evaluation of this property propagates through subsequent analyses with eventual consequences that are greatest for nighttime. It is not intended to recommend specific alternatives, but to demonstrate that such alternatives do indeed exist.

Daytime data presented here indicate that in daytime a value of $kB^{-1} \approx 2$ is appropriate, as recommended by Garratt and Francey (1978). At night, there is no apparent relationship between kB^{-1} and Re_* , except for the case of data collected over an arid site in a similarly arid landscape during a dry season experiencing minimal precipitation. For this dry season case, an assumption that kB^{-1} does not vary, on the average, with time of day seems appropriate. However, in other situations the scatter of results collected at night prohibits easy interpretation. In general, published relationships between kB^{-1} and Re_* can be simulated using random numbers, indicating that in the atmospheric case the assumptions made in some

numerical models are not good representations of the associations but are consequences of the shared variable syndrome.

The available data indicate that the scatter associated with kB^{-1} is largely due to uncertainties associated with the exchange of heat, with the role played by momentum exchange formulated better. In this latter context, consideration of the friction coefficient as an index of surface roughness provides a simpler path for simulating air–surface momentum exchange than does a more conventional approach based on tabulated or assumed roughness lengths. The friction coefficient C_f is a well-known property of the surface, depending on the logarithm of the familiar roughness length, and so varies less widely than does z_0 . In the context of a varying landscape, specification of an appropriate spatial average is a complicated task when based on assumptions about the roughness length, but becomes more straightforward when the different parts of the same landscape are characterized in terms of C_f .

The potential benefits of utilizing a thermal equivalent to C_f , the Stanton number St or the turbulent Stanton number St_* , are debatable. The data considered here indicate that daytime unstable and night-time stable regimes could be formulated in terms of different “plateau” values, if the site is suitably representative of the surrounding landscape. In reaching this conclusion, the variability around dusk and dawn has been discounted, since evaluation of St and St_* at such times is highly influenced by the low values of the temperature gradients and sensible heat fluxes. In applications of these results, it is expected therefore that the two-plateau assumption might be an appropriate first-order approximation, with a simple interpolation to reflect the changes at dusk and dawn.

The discussion of Stanton numbers and friction coefficients given here is intended to demonstrate that there are indeed alternatives to the way in which conventional mesoscale, regional and prognostic models are constructed. Instead of relying on classical micrometeorological expressions involving ethereal properties such as roughness lengths and displacement heights, it appears possible that simpler representations such as those suggested here might suffice. A more detailed discussion of these alternatives, and in particular of the potential role of the turbulent Stanton number, is given by Garratt (1992). On the basis of the data now examined, the nocturnal case might be better addressed using the observation (perhaps site-specific) that eddy fluxes of heat and momentum are well correlated at night.

These conclusions are based on a limited set of data, and obviously require additional attention. In particular, data obtained over tall crops and forests need to be considered. The discussion here about the causes of variability through dusk and dawn could be amenable to examination using data from a number of earlier experiments. If the present conclusions are justified, then it would seem appropriate to disregard the scatter surrounding these periods and to evaluate the most probable atmospheric behaviour using an interpolation of daytime and night-time regimes. The consequences of these conclusions on assumptions about requisite or optimal spatial and temporal averaging times remain to be examined.

Acknowledgements The ZIM data used were derived in an investigation of the exchange characteristics of several alternative agricultural practices in sub-Saharan Africa. The focus of the research program has been on CO_2 exchange; the work is partially funded by the U. S. Agency for International Development SANREM CRSP. The collaboration of staff of the International Maize and Wheat Improvement Centre (CIMMYT), Mount Pleasant, Harare, Zimbabwe (Director: Dr. Christian Thierfelder) is greatly appreciated. The BAMA data were obtained as a contribution to NOAA’s Convective Initiation field program. Thanks are belatedly due to Dr. Paul Frenzen, who coined the term “quasi-laminar layer” to draw attention to some of the fundamental difficulties of describing the processes of air–surface exchange.

Open Access This article is distributed under the terms of the Creative Commons Attribution 4.0 International License (<http://creativecommons.org/licenses/by/4.0/>), which permits unrestricted use, distribution, and reproduction in any medium, provided you give appropriate credit to the original author(s) and the source, provide a link to the Creative Commons license, and indicate if changes were made.

References

- Brutsaert W (1975) A theory for local evaporation (or heat transfer) from rough and smooth surfaces at ground level. *Water Resour Res* 11:543–550
- Brutsaert W (1982) *Evaporation into the atmosphere*. D. Reidel, New York
- Chamberlain AC (1966) Transfer of gases to and from grass and grass-like surfaces. *Proc Roy Soc A* 290:236–265
- Chamberlain AC (1968) Transfer of gases to and from surfaces with bluff and wave-like roughness elements. *Q J R Meteorol Soc* 94:318–332
- Chamberlain AC (1974) Mass transfer to bean leaves. *Boundary-Layer Meteorol* 6:477–486
- Chen Y, Yang K, Dzou D, Qin J, Guo X (2010) Improving the Noah land surface model in arid regions with a appropriate parameterization of the thermal roughness length. *J Hydrometeorol* 11:995–1006
- Gallagher MW, Beswick KM, Duyzer J, Westrate H, Choularton TW, Hummelshoj P (1997) Measurements of aerosol fluxes to Speulder forest using a micrometeorological technique. *Atmos Environ* 31:359–373
- Garland JA (2001) On the size dependence of particle deposition. *Water Air Soil Pollut Focus* 1:323–332
- Garratt JR (1992) *The atmospheric boundary layer*. Cambridge University Press, Cambridge
- Garratt JR, Hicks BB (1973) Momentum, heat and water vapour transfer to and from natural and artificial surfaces. *Q J R Meteorol Soc* 99:680–687
- Garratt JR, Francey RJ (1978) Bulk characteristics of heat transfer in the unstable, baroclinic boundary layer. *Boundary-Layer Meteorol* 15:399–421
- Garratt JR, Hicks BB, Valigura RA (1993) Comments on “The roughness length for heat and other vegetation parameters for a surface of short grass” by Duynkerke (1993: *J Appl Meteorol* 31:579–586). *J Appl Meteorol* 32:1301–1303
- Gong J, Wahba G, Johnson DR, Tribbia J (1998) Adaptive tuning of numerical weather prediction models: simultaneous estimation of weighting, smoothing, and physical parameters. *Mon Weather Rev* 126:210–231
- Hicks BB (1978) Some limitations of dimensional analysis and power laws. *Boundary-Layer Meteorol* 14:567–569
- Hicks BB, O’Dell DB, Eash NS, Sauer T (2015) Nocturnal intermittency in surface CO₂ concentrations in sub-Saharan Africa. *Agric For Meteorol* 200:129–134
- Hicks BB, Saylor RD, Baker BD (2016) Dry deposition of particles to canopies: a look back and the road forward. *J Geophys Res Atmos*. <https://doi.org/10.1002/2015JD024742>
- Kanda M, Kanega M, Kawai T, Moriwaki R (2007) Roughness lengths for momentum and heat derived from outdoor urban scale models. *J Appl Meteorol* 46:1067–1079
- Malhi Y (1996) The behaviour of the roughness length for temperature over heterogeneous surfaces. *Q J R Meteorol Soc* 122:1095–1125
- Marzban C, Sandgathe S, Doyle JD (2014) Model tuning with canonical correlation analysis. *Mon Weather Rev* 142:2018–2027
- O’Dell D, Sauer TJ, Hicks BB, Thierfelder C, Lambert DM, Logan J, Eash NS (2015) A short-term assessment of carbon dioxide fluxes under contrasting agricultural and soil management practices in Zimbabwe. *J Agric Sci* 7:32. <https://doi.org/10.5539/jas.v7n3p32>
- Owen PR, Thomson WR (1963) Heat transfer across rough surfaces. *J Fluid Mech* 15:321–334
- Pendergrass WR, Meyers TP, White R (2017) ATDD convective initiation program T-Profiler observations, Belle Mina, Alabama. NOAA technical report OAR ARL-271, 60 pp
- Plate EJ (1971) Aerodynamic characteristics of atmospheric boundary layers. US Atomic Energy Commission Critical Review TID-25465. Oak Ridge Division of Technical Information, Tennessee
- Paulson CA (1970) The mathematical representation of wind speed and temperature in the unstable atmospheric surface layer. *J Appl Meteorol* 9:857–861
- Stewart JB, Kustas WP, Humes KS, Nichols WD, Moran MS, de Bruin HAR (1994) Sensible heat flux-radiometric surface temperature relationship for eight semi-arid areas. *J Appl Meteorol* 33:1110–1117
- Verhoef A, de Bruin HAR, van den Hurk BJJM (1997) Some practical notes on the parameter kB^{-1} for sparse vegetation. *J Appl Meteorol* 36:560–572

- Yang K, Koike T, Hirohilo I, Kim J, Li X, Liu H, Liu S, Ma Y, Wang J (2008) Turbulent flux transfer over bare-soil surface characteristics and parameterization. *J Appl Meteorol* 47:276–290
- Zhang L, Gong S, Padro J, Barrie L (2001) A size-segregated particle dry deposition scheme for an atmospheric aerosol module. *Atmos Environ* 35:549–560